Available online at www.sciencedirect.com
SCIENCE DIRECT®
Journal of Sound and Vibration 289 (2006) 192–209
JOURNAL OF SOUND AND VIBRATION
www.elsevier.com/locate/jsvi

Generation of low-frequency vibration using a cantilever beam for calibration of accelerometers

Won-Suk Ohm*, Lixue Wu, Peter Hanes, George S.K. Wong

Acoustical Standards, Institute for National Measurement Standards, National Research Council, M-36, 1200 Montreal Road, Ottawa, Ont., Canada K1A 0R6

Received 8 July 2004; received in revised form 18 January 2005; accepted 3 February 2005
Available online 31 March 2005

Abstract

At low frequencies (below 10 Hz), performance of a conventional shaker is limited by small acceleration amplitudes and a high level of total harmonic distortion. The present article describes a low-frequency vibration generator that overcomes these limitations. The vibration generator consists of a cantilever beam excited by a conventional shaker. The cantilever beam is tuned to resonate at the desired excitation frequency, which leads to a relatively large vibratory motion at the beam tip with very small harmonic distortion. Analysis of the system is performed by means of model equations describing both the flexural and longitudinal components of vibration. A comprehensive measurement of the generator's performance confirms that it can serve as an economically attractive alternative to existing low-frequency vibration generators used in vibration measurement and calibration.

1. Introduction

Growing demands for low-frequency (below 10 Hz) vibration measurement have created a need for an accurate, robust, and economical means to calibrate vibration transducers at low frequencies [1]. The challenge of low-frequency vibration calibration oftentimes lies in generating low-frequency sinusoidal motion with good waveform purity. Typically, the requirements for a

*Corresponding author. Tel.: +1 613 993 1003; fax: +1 613 952 1394.
E-mail address: wonsuk.ohm@nrc-cnrc.gc.ca (W.-S. Ohm).

0022-460X/$ - see front matter © 2005 Elsevier Ltd. All rights reserved.
doi:10.1016/j.jsv.2005.02.002

Nomenclature

a	$\sqrt{EI/\rho A}$, parameter in flexural wave equation, $m^2\,s^{-1}$
$\bar{a}_v$	relative amplitude of transverse/rocking acceleration, in fraction
A	beam cross-sectional area, m^2
c_1	damping coefficient at first resonance frequency, Pa s
c_l	$\sqrt{E/\rho}$, longitudinal wave speed, $m\,s^{-1}$
$c(\omega)$	frequency-dependent damping coefficient, Pa s
E	Young's modulus of beam material, Pa
f	excitation frequency, Hz
f_1	first resonance frequency, Hz
$F_{d,s}$	amplitudes of dynamic and static parts of driving force, N
$F_{u,y}$	external forces in longitudinal and flexural directions, N
$H(x)$	Heaviside unit step function
i	$\sqrt{-1}$, imaginary unit
I	moment of inertia of beam cross-section, m^4
J	integral of Lagrangian density
l	beam length, m
$\mathscr{L}$	Lagrangian density, N
m	end mass, kg
$\bar{m}$	$m\beta/\rho A$, dimensionless end mass
r	$\sqrt{I/A}$, radius of gyration, m
s	coordinate along centroidal plane, m
$\bar{S}_{v,r}$	transverse sensitivity of reference transducer, %
$\bar{S}_{v,t}$	transverse sensitivity of test transducer, %
t	time, s
THD	total harmonic distortion, in fraction
u	longitudinal displacement, m
u_{THD}	uncertainty due to total harmonic distortion, %
u_v	uncertainty due to transverse/rocking vibration, %
x	material coordinate, m
x_0	position of driving force, m
y	flexural displacement, m
$y_{d,s}$	dynamic and static parts of flexural displacement, m
β	$\sqrt{\omega/a}$, flexural wave number for lossless beam, m^{-1}
β^*	$\beta[1+\mathrm{i}a^2\tilde{c}(\omega)/\omega]^{1/4}$, complex flexural wave number for lossy beam, m^{-1}
γ	damping exponent
δ	deviation of frequency response of test unit from that of reference transducer, %
δW_B	virtual work performed at boundaries
$\delta(x)$	Dirac delta function
ε	small ordering parameter
ε_{xx}	Green strain
θ	tangential angle, rad
κ	curvature, m^{-1}
λ	flexural wavelength, m
Π	$(\beta r)^2$, dimensionless beam thickness
ρ	density of beam material, $kg\,m^{-3}$
ω	angular excitation frequency, $rad\,s^{-1}$

vibration generator are specified in terms of (1) total harmonic distortion (THD) in acceleration, (2) transverse and rocking acceleration, (3) frequency and acceleration amplitude stability, and (4) hum and noise [2,3]. An electrodynamic shaker, when operated within its intended frequency range, can produce accurate vibratory motion meeting the above requirements. However, when calibrations are to be performed at low frequencies, the acceleration generated by a conventional shaker is relatively low in amplitude due to the limited maximum displacement, and is often subject to a high level of harmonic distortion. Under these circumstances, a vibration generator specifically tailored to produce low-frequency motion, such as a long-stroke shaker [1] or a dual centrifuge [4], may be required. Because of the specific mechanisms used to provide the required performance at low frequencies, such special-purpose vibration generators can be costly.

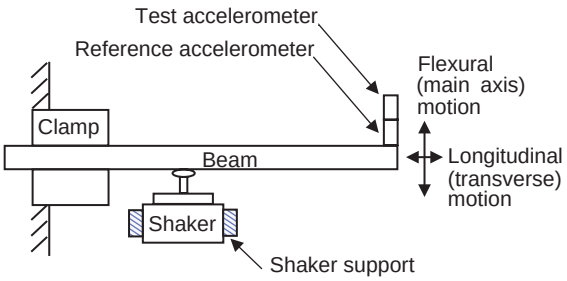

Fig. 1. Plan-view of the low-frequency vibration generation/calibration system.

This article presents a simple method for extending the effective low-frequency range of a conventional shaker. A cantilever beam, whose length is adjusted to yield the first resonance at the desired test frequency, is driven by a shaker, and provides selective excitation of the frequency component of interest (Fig. 1). The resulting flexural motion at the free end of the beam exhibits only small harmonic distortion despite the presence of harmonic components in the shaker's output. Although the technique has been used extensively in vibration and acoustics, no detailed accounts of its suitability for precision applications such as low-frequency vibration calibration appear to have been reported. The purpose of the article is to fill this void and to provide theoretical and experimental foundations for the use of the technique by laboratories that perform low-frequency accelerometer calibration.

The initial part of the article is devoted to an analysis of the forced vibration of a cantilever beam. Although there exists a plethora of literature on flexural vibration of an elastic beam, relatively little attention has been given to the longitudinal component of particle displacement arising from the flexion of a beam. Coupling between the flexural and longitudinal modes leads to the generation of a relatively small motion transverse to the main-axis component, whose level is of prime concern for use of the cantilever beam as a vibration generator in accelerometer calibration. (For the setup shown in Fig. 1, the flexural component of beam displacement is considered as the "main-axis" motion, while the longitudinal component that is normal to the main axis is referred to as the "transverse" motion.) Therefore, a set of model equations describing both the flexural and the associated longitudinal displacements of an elastic beam are considered. Beam motion at the free end is illustrated in the form of frequency response, acceleration-time profile, and particle trajectory.

Various aspects of the performance of the vibration generator, such as total harmonic distortion and transverse/rocking acceleration, are measured in the frequency range from 2 to 10 Hz and in the acceleration range from 1 to 10 $m\,s^{-2}$. The influence of the vibration generator on the measurement uncertainty associated with the comparison calibration of accelerometers is also addressed.

2. Theory

Consider a schematic view of an elastic beam shown in Fig. 2(a). An initially straight, isotropic, homogeneous beam of a constant rectangular cross-section is assumed. The deflection of the beam

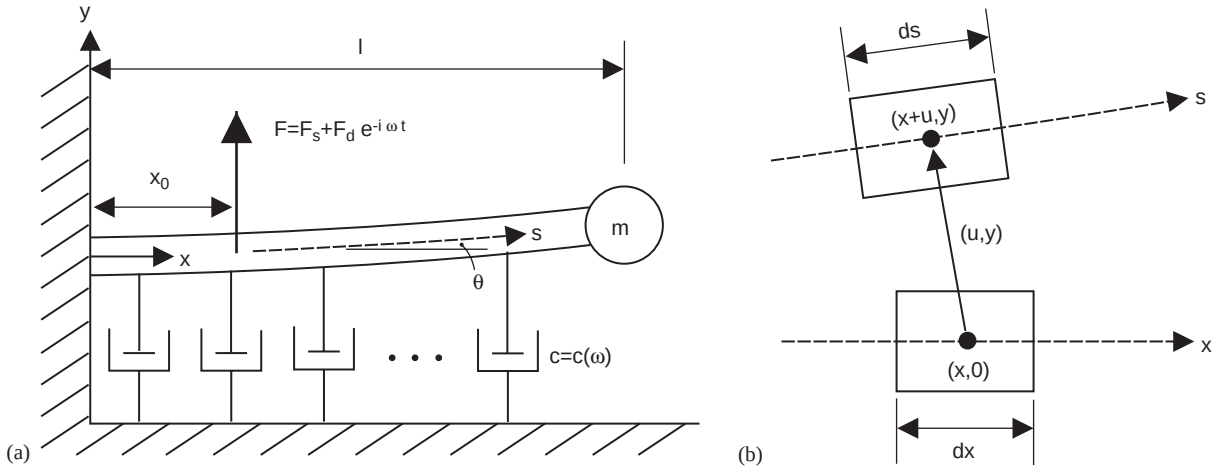

Fig. 2. (a) Schematic model of the low-frequency vibration generator and (b) flexural and longitudinal displacements of an infinitesimal beam element.

is represented by that of the centroidal plane (shown in dashed line). The material coordinate x coincides with the position of the centroidal plane prior to deformation. The flexural and associated longitudinal displacements of an infinitesimal element are denoted by y and u, respectively [Fig. 2(b)]. To characterize the relative magnitudes of the flexural and longitudinal components of motion, a small ordering parameter denoted by ε is introduced. Under the current ordering scheme, the flexural displacement, when normalized by a characteristic flexural wavelength λ, is of $O(\varepsilon)$ smallness [$y/\lambda \sim O(\varepsilon)$]. The longitudinal motion due to the flexion of a beam is deemed to be a second-order effect [$u/\lambda \sim O(\varepsilon^2)$], which is consistent with experimental observations. The force exerted by a shaker is represented by $F = F_s + F_d e^{-i\omega t}$ at $x = x_0$, where ω is the excitation frequency and $F_{s,d}$ are the amplitudes of the static and dynamic parts of the shaker force, respectively. (The purpose of the static load F_s is to model the constant shaker force that is required to maintain a steady contact between the shaker tip and the beam.) The system damping is modeled by a viscous foundation [5,6] with frequency-dependent damping coefficient $c(\omega)$. For derivation of boundary conditions at the free end ($x = l$), vibration pickups and mounting fixtures are assumed to possess negligible rotational inertia and are collectively represented by the end mass m. The equation of motion and its boundary conditions describing the flexural motion at $O(\varepsilon)$ are

$$\frac{\partial^4 y}{\partial x^4} + \tilde{c}(\omega)\frac{\partial y}{\partial t} + \frac{1}{a^2}\frac{\partial^2 y}{\partial t^2} = \tilde{F}_s \delta(x - x_0) + \tilde{F}_d \delta(x - x_0) e^{-i\omega t}, \tag{1}$$

$$y(0,t) = \frac{\partial y(0,t)}{\partial x} = \frac{\partial^2 y(l,t)}{\partial x^2} = 0, \tag{2}$$

$$m\frac{\partial^2 y(l,t)}{\partial t^2} = EI\frac{\partial^3 y(l,t)}{\partial x^3}, \tag{3}$$

where $a = \sqrt{EI/\rho A}$, E Young's modulus of the beam material, I the moment of inertia of the cross-section, ρ the density, A the cross-sectional area, $\delta(x)$ the Dirac delta function, $\tilde{c}(\omega) = c(\omega)/EI$, and $\tilde{F}_{s,d} = F_{s,d}/EI$. Accordingly, the associated longitudinal motion at $O(\varepsilon^2)$ is described by

$$\frac{\partial^2 u}{\partial x^2} = -\frac{1}{2}\frac{\partial}{\partial x}\left(\frac{\partial y}{\partial x}\right)^2, \tag{4}$$

$$u(0,t) = 0, \tag{5}$$

$$m\frac{\partial^2 u(l,t)}{\partial t^2} = -EA\frac{\partial u(l,t)}{\partial x} - \frac{EA}{2}\left[\frac{\partial y(l,t)}{\partial x}\right]^2. \tag{6}$$

Derivations of the above equations of motion [Eqs. (1) and (4)] are found in Appendix A.

Three notable features are observed regarding the above boundary value problem (1)–(6). First, coupling between the flexural and longitudinal modes occurs through the terms

$$-\frac{1}{2}\frac{\partial}{\partial x}\left(\frac{\partial y}{\partial x}\right)^2 \quad \text{and} \quad -\frac{EA}{2}\left[\frac{\partial y(l,t)}{\partial x}\right]^2$$

in Eqs. (4) and (6), i.e., the longitudinal motion is excited by the forcing functions that depend quadratically on the flexural-wave solution. The solution procedure thus requires the flexural-wave solution be obtained, which is then substituted into Eqs. (4) and (6). Second, the longitudinal-component equation (4) indicates that the centroidal plane of a beam undergoes uniform extensional deformation. [See the discussion leading to Eqs. (A.1) and (A.2) in Appendix A.] Third, the presence of an end mass leads to time-dependent boundary conditions (3) and (6), for which normal modes do not form an orthogonal set. Because the conventional normal mode expansion fails to produce solutions for this type of boundary value problem, other means of analysis [7–9] are in order.

The Laplace transform [9] is used to seek the flexural-wave solution. The static deflection in response to static load is given by

$$y_s(x) = \tilde{F}_s[\tfrac{1}{2}x_0x^2 - \tfrac{1}{6}x^3 + \tfrac{1}{6}(x-x_0)^3H(x-x_0)], \tag{7}$$

where $H(x)$ is the Heaviside unit step function. The dynamic part of the solution is cast in the form $y_d(x,t) = Y(x)e^{-i\omega t}$, where applying the Laplace transform yields

$$Y(x) = \frac{\tilde{F}_d}{(\beta^*)^3}\left[\frac{N_1M(x)}{D} + \frac{N_2L(x)}{D} + H(x-x_0)L(x-x_0)\right]. \tag{8}$$

Here,

$$\beta^* = [\beta^4 + i\omega\tilde{c}(\omega)]^{1/4} \approx \beta\left[1 + i\frac{a^2\tilde{c}(\omega)}{4\omega}\right] \tag{9}$$

is the wave number for a lossy beam and $\beta = \sqrt{\omega/a}$ the lossless wave number. Functions $L(x)$ and $M(x)$ are defined by

$$L(x) = \frac{\sinh\beta^*x - \sin\beta^*x}{2}, \quad M(x) = \frac{\cosh\beta^*x - \cos\beta^*x}{2}. \tag{10,11}$$

Coefficients N_1, N_2, and D are given by

$$N_1 = L'''(l)L''(l-x_0) - L''(l)L'''(l-x_0) + \left(\frac{m\omega^2}{EI}\right)[L(l)L''(l-x_0) - L''(l)L(l-x_0)], \tag{12}$$

$$N_2 = L'''(l-x_0)M''(l) - L''(l-x_0)M'''(l) + \left(\frac{m\omega^2}{EI}\right)[L(l-x_0)M''(l) - L''(l-x_0)M(l)], \tag{13}$$

$$D = L''(l)M'''(l) - L'''(l)M''(l) + \left(\frac{m\omega^2}{EI}\right)[L''(l)M(l) - L(l)M''(l)]. \tag{14}$$

The complete flexural-wave solution then has the form

$$y(x,t) = y_s(x) + \mathrm{Re}[Y(x)\mathrm{e}^{-\mathrm{i}\omega t}] = y_s(x) + Y_R(x)\cos\omega t + Y_I(x)\sin\omega t, \tag{15}$$

where $Y_R(x)$ and $Y_I(x)$ are the real and imaginary parts of $Y(x)$, respectively. Resonance occurs when the determinant $|D|$ takes the minimum value (or for a lossless beam, $D = 0$). Setting $D = 0$ thus results in the characteristic equation for a lossless cantilever beam, that is,

$$1 + \cosh\beta l\cos\beta l + \overline{m}[\cos\beta l\sinh\beta l - \sin\beta l\cosh\beta l] = 0, \tag{16}$$

where $\overline{m} = m\beta/\rho A$ is the dimensionless end mass.

Direct integration of Eq. (4), following the substitution of Eq. (15), yields the longitudinal-wave solution:

$$\begin{aligned} u(x,t) = & -\frac{1}{4}\int_0^x [2(y_s')^2 + (Y_R')^2 + (Y_I')^2]\,\mathrm{d}\xi \\ & - \int_0^x y_s' Y_R'\,\mathrm{d}\xi\cos\omega t - \int_0^x y_s' Y_I'\,\mathrm{d}\xi\sin\omega t \\ & - \frac{1}{4}\int_0^x [(Y_R')^2 - (Y_I')^2]\,\mathrm{d}\xi\cos 2\omega t - \frac{1}{4}\int_0^x (2Y_R'Y_I')\,\mathrm{d}\xi\sin 2\omega t \\ & + \left[\frac{\omega^2}{\omega^2 - (EA/lm)}\right]\int_0^l y_s' Y_R'\,\mathrm{d}\xi\left(\frac{x}{l}\right)\cos\omega t \\ & + \left[\frac{\omega^2}{\omega^2 - (EA/lm)}\right]\int_0^l y_s' Y_I'\,\mathrm{d}\xi\left(\frac{x}{l}\right)\sin\omega t \\ & + \frac{1}{4}\left[\frac{(2\omega)^2}{(2\omega)^2 - (EA/lm)}\right]\int_0^l [(Y_R')^2 - (Y_I')^2]\,\mathrm{d}\xi\left(\frac{x}{l}\right)\cos 2\omega t \\ & + \frac{1}{4}\left[\frac{(2\omega)^2}{(2\omega)^2 - (EA/lm)}\right]\int_0^l (2Y_R'Y_I')\,\mathrm{d}\xi\left(\frac{x}{l}\right)\sin 2\omega t, \end{aligned} \tag{17}$$

where primes on $y_s(\xi)$ and $Y_{R,I}(\xi)$ denote differentiation with respect to the integration variable ξ. Examination of Eq. (17) reveals that, due to the quadratic nature of flexural–longitudinal mode

coupling, the longitudinal response consists of terms oscillating at both the excitation frequency ω and twice that frequency, 2ω. Notice that the terms oscillating at ω in Eq. (17) originate from the static load F_s; if $F_s = 0$ (and therefore $y_s = 0$), the longitudinal mode responds solely at frequency 2ω. The last four terms in Eq. (17) constitute the dynamic response of a spring–mass oscillator, wherein the beam behaves as a lumped spring element with spring constant EA/l in the longitudinal direction. Because the frequency range of interest lies well below the resonance frequency of the oscillator, these four terms are negligible.

3. System implementation

The NRC low-frequency vibration generator consists of an annealed brass beam of dimensions 50.8 mm × 3.2 mm × 1676.4 mm ($2'' \times 1/8'' \times 66''$), an electrodynamic shaker (model EA1250, MB Electronics), and a power amplifier (model 2125 MB, MB Electronics). The beam is mounted on a rig equipped with a clamp, which enables the effective beam length l to be adjusted. The beam length is chosen such that the first resonant mode of vibration occurs at the desired excitation frequency. Given the beam cross-sectional dimensions (50.8 mm × 3.2 mm), the material constants for brass [10] ($\rho = 8500\,\mathrm{kg\,m^{-3}}$ and $E = 104\,\mathrm{GPa}$), an excitation frequency ω, and an end mass m, the characteristic equation (16) can be solved for the beam length l that gives rise to the first resonance. In practice, an approximate equation for the beam length is used

$$l = (1.8751154 - 1.00098\overline{m} + 0.748624\overline{m}^2 - 0.44818\overline{m}^3 + 0.174145\overline{m}^4 - 0.031497\overline{m}^5)/\beta, \tag{18}$$

whose results deviate from those obtained from Eq. (16) by no more than 6 ppm in the range $0 \leqslant \overline{m} \leqslant 1$. (For example, the beam length at 2 Hz, assuming an end mass of 45 g, is obtained by substituting the corresponding parameters $\beta = 1.9721\,\mathrm{m^{-1}}$ and $\overline{m} = 0.0642$ into Eq. (18); the result is $l = 920$ mm.) Subsequent fine-adjustment of the beam length may be necessary to achieve the lowest level of total harmonic distortion.

Some nonlinear effects specific to a cantilever system should be minimized to attain good waveform purity. To suppress the loss-of-contact nonlinearity [11], it is imperative to pre-load the beam with the shaker tip and to ensure a steady contact during the motion. The influence of higher resonant modes on the first mode via nonlinear interaction [12] can be reduced by placing the shaker tip at the node of a higher vibration mode and therefore preventing it from being excited. However, this scheme may lead to the loss-of-contact nonlinearity mentioned above due to the limited excursion of the shaker tip; the first node of the third mode, for example, is almost half the beam length away from the clamped end, where the vibration amplitude of the first mode is so large that the shaker tip and the beam are no longer able to maintain a steady contact. A practical approach is to place the shaker close to the clamped end and to use a moderate excitation force such that the beam displacement is large enough for the purpose of vibration calibration, but is not too large to trigger the nonlinear coupling of higher vibration modes. In our setup, the shaker tip is situated 104 mm away from the clamped end.

Two different types of accelerometers are used in conjunction with a conditioning amplifier (model 2650, Brüel & Kjær) to measure vibration; a general-purpose, uniaxial accelerometer

(model 4382, Brüel & Kjær) is used for most of the vibration measurements, while a triaxial accelerometer (model 4321, Brüel & Kjær) is employed for the simultaneous measurement of main-axis and transverse acceleration. Accelerometers are mounted such that their main sensitivity axes are aligned in the direction of flexural motion. Output from an accelerometer is displayed on an oscilloscope (model TDS724D, Tektronix) as a time waveform and on a digital voltmeter (model 1271, Datron) as rms voltage. For measurements of the shaker force, a force transducer (model 209B12, PCB Piezotronics) can be inserted at the contact point of the shaker and the beam. Frequency of the vibration is measured with a frequency counter (model PM6680B, Fluke).

4. Results

4.1. Beam motion at the free end

To illustrate the beam motion at the free end, a beam that is tuned to have its first resonance at 2 Hz ($l = 920$ mm) is considered. Fig. 3(a) shows the computed frequency response in flexural acceleration (solid line) compared with measurements (circles). For measurement of the frequency response, sinusoidal force with constant amplitude $F_d = 4.6$ N is applied over the frequency range of interest and the corresponding flexural acceleration is measured with a uniaxial accelerometer (model 4382, Brüel & Kjær). A frequency-power law for the system damping,

$$\tilde{c}(f) = \tilde{c}_1 \left(\frac{f}{f_1}\right)^{\gamma}, \tag{19}$$

is assumed, where the damping coefficient $\tilde{c}_1$ at the first resonance frequency f_1 and the exponent γ are determined empirically in such a way as to yield the best fit with measurements. (For the beam

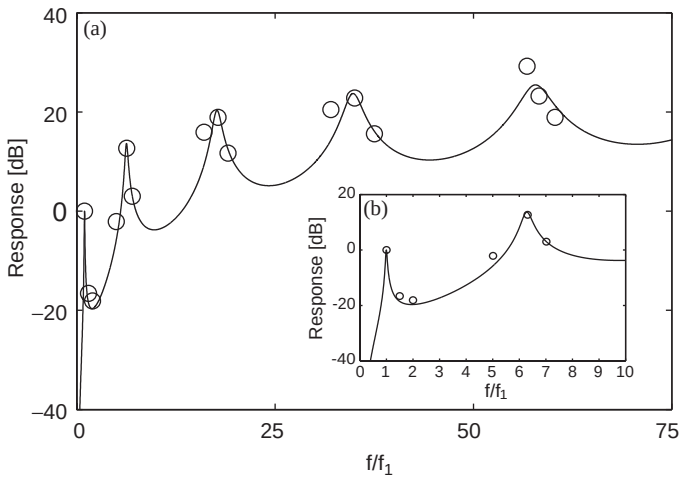

Fig. 3. Frequency response in flexural acceleration at the beam tip. Acceleration and frequency are normalized to the corresponding values at the first resonance. Solid line: calculation, circles: measurements. Each measurement point represents an average over five readings.

under consideration with $f_1 = 2\,\text{Hz}$, these values are $\tilde{c}_1 = 8 \times 10^{-2}\,\text{m}^{-4}\,\text{s}$ and $\gamma = 1$.) Shown in the inset of Fig. 3(b) is an expanded view of the frequency response for frequencies up to the second resonant peak.

Measurements of acceleration profile at 2 Hz (solid lines), taken with the aid of a triaxial accelerometer (model 4321, Brüel & Kjær), are displayed along with computations (dashed lines) in Figs. 4 and 5. A shaker force with amplitudes $F_s = 30\,\text{N}$ and $F_d = 17.7\,\text{N}$ is applied. As for the flexural acceleration, Fig. 4 shows good agreement between measured (solid line) and computed (dashed line) waveforms. However, Fig. 5 shows that the theory (dashed line) overestimates the longitudinal component of acceleration. The discrepancy can in part be attributed to the rocking motion of the accelerometer-mounting surface (and subsequent tilting of the accelerometer axes)

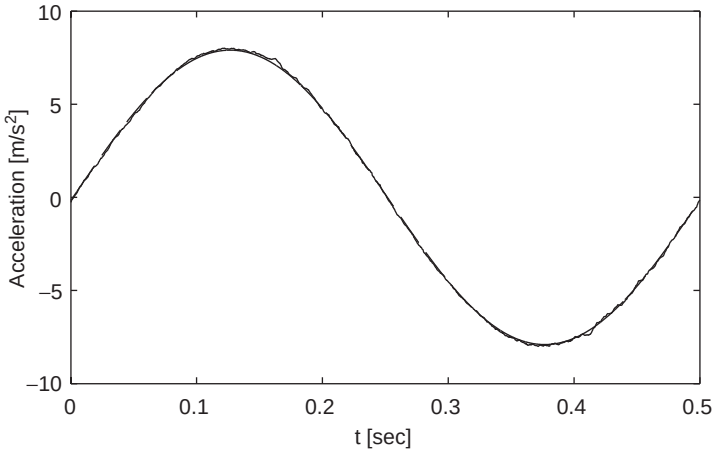

Fig. 4. Flexural acceleration at the beam tip. Measured (solid line) and calculated (dashed line) waveforms are virtually indistinguishable.

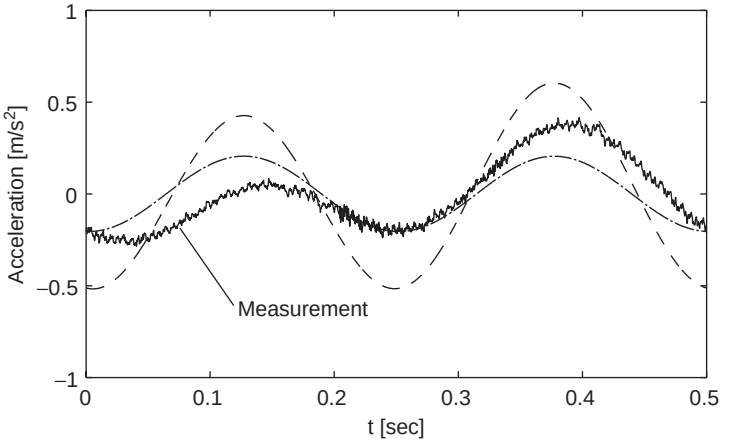

Fig. 5. Longitudinal acceleration at the beam tip. The measured waveform (solid line) is compared with calculations: dashed line, longitudinal only; dash-dot line, longitudinal and rotational.

resulting from beam flexion. To account for the effect of rocking motion on acceleration measurements, vector decomposition of acceleration $\ddot{\mathbf{r}}$ is undertaken in the coordinate system spanned by the accelerometer axes:

$$\ddot{\mathbf{r}} = \begin{pmatrix} \cos\theta & \sin\theta \\ -\sin\theta & \cos\theta \end{pmatrix} \begin{pmatrix} \ddot{u} \\ \ddot{y} \end{pmatrix} = \begin{pmatrix} \ddot{u}\cos\theta + \ddot{y}\sin\theta \\ \ddot{y}\cos\theta - \ddot{u}\sin\theta \end{pmatrix} = \begin{pmatrix} \ddot{u} + \ddot{y}y' + O(\varepsilon^4) \\ \ddot{y} + O(\varepsilon^3) \end{pmatrix}, \tag{20}$$

where θ is the tangential (or tilt) angle of the mounting surface. In the above equation, the terms $\ddot{y}$ and $\ddot{u} + \ddot{y}y'$ represent, respectively, the flexural and longitudinal accelerations that are apparent to an accelerometer. Eq. (20) indicates that at the leading order [$O(\varepsilon)$], rocking of the mounting surface does not influence the measurement of the main-axis (flexural) acceleration. Instead, the effect of rocking vibration $\ddot{y}y'$ is combined with that of the transverse (longitudinal) vibration $\ddot{u}$ to form a much smaller $O(\varepsilon^2)$ effect, represented by the terms $\ddot{u} + \ddot{y}y'$. It can be seen in Fig. 5 that the combination $\ddot{u} + \ddot{y}y'$ (dash-dot line) shows better agreement with the measured acceleration (solid line) than the longitudinal acceleration $\ddot{u}$ alone (dashed line). The high-frequency wiggles observed in the measured waveform are due to the hum and noise whose spectral peaks are at the integer multiples of 60 Hz.

Fig. 6 shows the displacement of the beam tip at 2 Hz, calculated from Eqs. (15) and (17). In Fig. 6(a), the flexural and longitudinal components are plotted on different amplitude scales because of the order-of-magnitude difference in their nominal amplitudes. The trajectory of the beam tip is shown in Fig. 6(b). Note that the presence of 2ω-terms in the longitudinal displacement [recall Eq. (17)] manifests itself as the slight curvature of the trajectory; if the

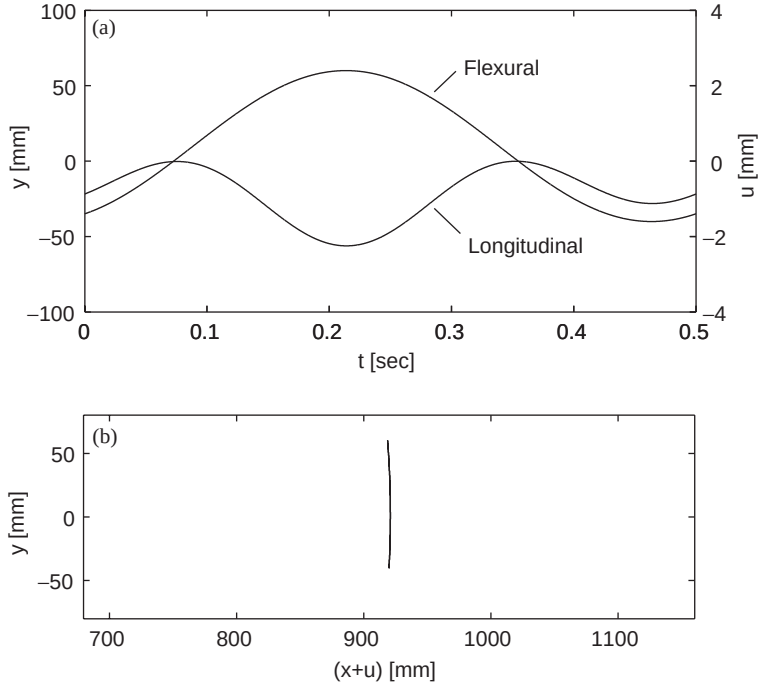

Fig. 6. Computed (a) displacement and (b) trajectory of the beam tip.

longitudinal mode responded only at the excitation frequency ω, as in the case of the flexural mode, the trajectory would have been a straight line.

4.2. Generator performance

A comprehensive set of measurements is undertaken regarding the performance of the low-frequency vibration generator. Note that we present here only the frequency and amplitude information because phase measurements are seldom performed in vibration calibration unless the transducers under test are to be used in an array configuration. In Table 1 the results are listed at three different levels of nominal acceleration for each of five test frequencies. Short-term frequency stability is obtained by computing the repeatability (defined as the relative standard deviation of the mean [13]) of readings from the frequency counter over a period of one minute. Similarly, acceleration amplitude stability is given by the repeatability of rms voltage readings from the voltmeter. Both frequency and acceleration amplitude stability generally improve with increasing level of acceleration because of the enhanced signal-to-noise ratio at higher acceleration levels.

The spectrum analyzer function of the oscilloscope (model TDS724D, Tektronix) is used to assess the total harmonic distortion in acceleration, where the first ten harmonic components are included in the calculation. [It is necessary to consider up to the tenth harmonic because it is likely that the sixth and seventh harmonics, located near the second resonant peak of the frequency

Table 1
Performance of the low-frequency vibration generator

Frequency (Hz) (Beam length)	Acceleration (m/s^2)	Frequency stability (ppm)	Acceleration amplitude stability (ppm)	THD (%)	Transverse and rocking vibration (%)	Level of hum and noise below full output (dB)
2	1	431	4271	0.7	5.0	
(920 mm)	5	88	558	0.7	2.8	51
	10	60	1104	1.3	4.1	
4	1	361	1155	0.6	2.7	
(642 mm)	5	13	575	0.5	2.8	52
	10	7	273	0.9	3.0	
5	1	36	1989	0.7	3.2	
(571 mm)	5	12	632	0.5	3.2	50
	10	12	192	0.8	3.1	
8	1	19	1988	3.5	4.0	
(446 mm)	5	20	897	0.8	3.7	50
	10	3	183	0.9	3.7	
10	1	64	1765	4.5	4.9	
(396 mm)	5	19	324	1.3	4.1	51
	10	5	354	0.9	4.1	

Quantities in the parentheses in the first column specify beam lengths that yield the first resonance at the corresponding frequencies.

Table 2
Performance of the low-frequency vibration generator at acceleration levels $5\,m\,s^{-2}$ (for 2, 4, and 5 Hz) and $10\,m\,s^{-2}$ (for 8 and 10 Hz), shown with specifications in the ISO standards [2,3] for vibration calibration

	NRC low-frequency vibration generator	ISO 16063-11:1999 specification for primary calibration	ISO 16063-21:2003 specification (Example 1) for comparison calibration
Frequency stability (ppm)	$\leqslant 88$	<500	$\leqslant 1000$
Acceleration amplitude stability (ppm)	$\leqslant 632$	<500	$\leqslant 1000$
THD (%)	$\leqslant 0.9$	$\leqslant 2$	$\leqslant 10$
Transverse/rocking vibration (%)	$\leqslant 4.1$	<1	$\leqslant 10$
Level of hum and noise below full output (dB) ($f \geqslant 10$ Hz)	51	$\geqslant 70$	$\geqslant 50$
Level of hum and noise below full output (dB) ($f < 10$ Hz)	$\geqslant 50$	$\geqslant 70$	$\geqslant 20$

response of the beam, are amplified and thus degrade the overall performance. See Fig. 3(b) for an example.] As expected, the harmonic distortion of the generator is very small over the frequency and acceleration ranges of interest. Except for the cases of 8 and 10 Hz at the lowest acceleration level, all measured values of total harmonic distortion are well within the limit of 2% specified by the ISO standard describing primary vibration calibration [2]. Greater values of harmonic distortion are encountered for the cases of 8 and 10 Hz, because the second resonant mode of the beam (occurring near 60 Hz for these cases) is excited by hum and noise whose spectral peak is at 60 Hz. However, as the acceleration level increases, the improved signal-to-noise ratio leads to smaller total harmonic distortion.

Transverse and rocking accelerations are shown in terms of the ratio of their combined magnitude [represented by $\ddot{u} + \ddot{y}y'$ in Eq. (20)] to that of the main-axis acceleration. Table 1 shows that the transverse and rocking acceleration is sufficiently small (3–5%) for the comparison calibration of accelerometers, where the specified maximum for transverse/rocking vibration in the ISO standard [3] is 10%. Hum and noise, mainly generated by the power amplifier, is approximately 50 dB below the full output over the frequency range of interest.

To examine the overall suitability of the generator for vibration calibration, the performance at acceleration levels $5\,m\,s^{-2}$ (for 2, 4 and 5 Hz) and $10\,m\,s^{-2}$ (for 8 and 10 Hz) is compared with the requirements in the ISO standards [2,3] in Table 2. (The above combinations of frequencies and acceleration levels are deemed appropriate for calibration.) The generator fulfills all the requirements for comparison calibration.

5. Calibration of accelerometers

The vibration generator described above is used in a system for the comparison calibration of an accelerometer in the frequency range from 2 to 10 Hz. The reference and test transducers are mounted back-to-back at the free end of the beam (Fig. 1). Outputs from two transducers are fed into separate channels of a digital voltmeter and their rms voltage ratio is computed to yield the

sensitivity magnitude of the test transducer. The reference transducer set consists of a uniaxial accelerometer (model 4382, Brüel & Kjær) and a charge amplifier (model 2650, Brüel & Kjær). For a typical test accelerometer, the relative expanded uncertainty of the comparison calibration employing the cantilever-beam vibration generator is 2.6% at a confidence level of 95%. Some of the sources of measurement uncertainty arising from the vibration generator are discussed below.

5.1. Total harmonic distortion

As mentioned above, the sensitivity magnitude of the test accelerometer is given by the ratio of the rms voltages from the reference and test channels. Because total harmonic distortion adds incoherently to the fundamental component in both the reference and test channels, the relative uncertainty contribution u_{THD} due to total harmonic distortion can be written as

$$u_{\mathrm{THD}} = \frac{\sqrt{1 + [\mathrm{THD}\ (1+\delta)]^2}}{\sqrt{1+\mathrm{THD}^2}} - 1, \tag{21}$$

where THD is the total harmonic distortion and δ is the maximum deviation of the frequency response of the test transducer from that of the reference. A quick algebra involving binomial expansion of both the numerator and denominator in Eq. (21) yields

$$u_{\mathrm{THD}}[\%] = \mathrm{THD}^2 \cdot \delta, \tag{22}$$

where the values of THD and δ are given in fraction and percent, respectively.

Because of the low distortion levels of the vibration generator, the resulting contribution is less than 0.001% for $\delta = 10\%$ at the levels and frequencies used in the calibration. Assuming a rectangular probability distribution [13] (divisor $\sqrt{3}$), the relative standard uncertainty due to harmonic distortion is 0.0006%.

5.2. Transverse and rocking acceleration

The formula used to evaluate the influence u_v of transverse and rocking acceleration is [3]

$$u_v[\%] = \overline{a}_v \cdot \sqrt{\overline{S}_{v,r}^2 + \overline{S}_{v,t}^2}. \tag{23}$$

Here, $\overline{a}_v$ is the relative amplitude of transverse/rocking acceleration expressed in fraction and $\overline{S}_{v,r}$, $\overline{S}_{v,t}$, are, respectively, transverse sensitivities of the reference and test transducers in percent. (Maximum transverse sensitivity of 5% is assumed for both the reference and test transducers.) Transverse/rocking acceleration of the vibration generator composes the largest systematic effect (0.4%) in the overall uncertainty, other than those arising from the reference transducer set. The effect is assumed to have a special 1-σ distribution [3] (divisor $\sqrt{18}$) and thus the corresponding relative standard uncertainty is 0.1%.

5.3. Hum and noise

Hum and noise adds incoherently to the fundamental component in both the reference and test channels. Therefore, a formula similar to that employed in the calculation of distortion contribution [Eq. (22)] can be used to assess the uncertainty due to hum and noise; simply

substitute the relative magnitude of hum and noise given in fraction for the value of THD in Eq. (22). The uncertainty contribution is 0.001%. Assuming a rectangular probability distribution leads to a relative standard uncertainty of 0.0006%.

6. Conclusions

A system for generation of low-frequency vibration is presented. Resonance of a cantilever beam is harnessed in order to extend the effective frequency range of a conventional shaker below 10 Hz. Model equations that describe both the flexural and longitudinal motion of an elastic beam are derived for an analysis of the vibration generator. The generator performance is measured for a set of frequencies and acceleration levels of interest. Apart from the ease of implementation, the current vibration generator shows satisfactory performance, especially in terms of very low harmonic distortion. The generator meets all the requirements specified by the International Standard ISO 16063-21:2003 for comparison calibration of vibration transducers.

Acknowledgments

The present work was performed when the first author held an NSERC Canadian Government Laboratory Visiting Fellowship Award at the Institute for National Measurement Standards, National Research Council Canada.

Appendix A. Derivation of model equations

Model equations describing the flexural and the resulting longitudinal motion of an elastic beam are usually found in the literature that deals with the finite-amplitude vibration of a beam [14–22]. The longitudinal motion caused by beam flexion is coupled with the flexural component through nonlinear relations and constitutes a higher-order effect. Therefore, the geometric nonlinearity, which determines the coupling of the flexural and longitudinal modes, must be considered in the derivation. Geometric nonlinearity arises from two distinct mechanisms: (1) the Green strain relation [Eq. (A.1), to be discussed below] that quantifies extensional deformation of the centroidal plane of a beam and (2) the nonlinear curvature [Eq. (A.5), to follow] of the deflection curve. Depending on the treatment of the above nonlinear mechanisms, the existing literature on nonlinear beam vibration can be grouped into three categories. The first group of authors [14–16] employs the inextensibility assumption (i.e., the centroidal plane of a beam undergoes neither extension nor compression and thus the corresponding Green strain remains zero throughout the motion) and approximate expressions for nonlinear curvature that include both the flexural and longitudinal components. In the second group of work [17–19], derivations are performed specifically for a simply supported beam with negligible longitudinal inertia, where uniform extension of the centroidal plane is taken into account. Other investigators [20–22] consider the full extensibility of the centroidal plane with nonzero longitudinal inertia, but use linear approximation for the curvature.

Although varying in the level of complexity and sophistication, none of the aforementioned studies consider extensibility and the exact nonlinear curvature, simultaneously. In this regard, our aim here is to derive a set of model equations that accounts for geometric nonlinearity to the fullest extent. The derivation most closely follows that of Crespo da Silva and Glynn [15], but differs substantially in the following aspects. First, the present derivation does not employ any assumptions pertaining to the extensibility of the centroidal plane, whereas in the derivation of Crespo da Silva et al., the inextensibility condition is used as a "constraint" that leads to the creation of a somewhat fictitious external force represented by the Lagrangian multiplier λ. Second, the exact expression for nonlinear curvature is used, which does not appear in any of the aforementioned work.

We start with the Green strain ε_{xx}, associated with the elongation of the centroidal plane,

$$\varepsilon_{xx} = [u' + \tfrac{1}{2}(y')^2] + \tfrac{1}{2}(u')^2, \tag{A.1}$$

where primes denote differentiation with respect to the material coordinate x. The bracketed terms constitute the leading contribution at $O(\varepsilon^2)$, whereas the last term represents a much smaller $O(\varepsilon^4)$ effect. In the case of negligible longitudinal inertia, there is no wave motion along the centroidal plane and, therefore, the centroidal plane experiences uniform extensional strain that varies only in time. In mathematical terms, this is expressed as, at $O(\varepsilon^2)$,

$$\varepsilon_{xx} = u' + \tfrac{1}{2}(y')^2 = \varepsilon_{xx}(t). \tag{A.2}$$

Note that the inextensibility condition at $O(\varepsilon^2)$,

$$\varepsilon_{xx} = u' + \tfrac{1}{2}(y')^2 = 0, \tag{A.3}$$

is a special case of Eq. (A.2). The tangential angle θ of the deflection curve, as illustrated in Fig. 2(a), is related to the flexural and longitudinal displacements via

$$\tan\theta = \frac{y'}{1+u'}. \tag{A.4}$$

The exact expression for the nonlinear curvature κ is then given by [23]

$$\kappa = \frac{\mathrm{d}\theta}{\mathrm{d}s} = \frac{(1+u')y'' - u''y'}{[(1+u')^2 + (y')^2]^{3/2}}, \tag{A.5}$$

where s is the arc length measured along the centroidal plane [dashed line in Fig. 2(a)].

Simpler forms of the above equation have been used by some investigators, most notably, $\kappa \approx (1+u')y'' - u''y'$ by Wagner [14] and

$$\kappa \approx \frac{(1+u')y'' - u''y'}{(1+u')^2 + (y')^2}$$

by Crespo da Silva et al. [15].

To obtain equations of motion from Hamilton's principle, the Lagrangian density of the system needs to be considered. For a Bernoulli–Euler beam, the Lagrangian density $\mathscr{L}$ containing translational and rotational inertia, and strain energy due to extension and bending, reads

$$\mathscr{L} = \tfrac{1}{2}\rho A(\dot{u}^2 + \dot{y}^2) + \tfrac{1}{2}\rho I\dot{\theta}^2 - \tfrac{1}{2}EA\varepsilon_{xx}^2 - \tfrac{1}{2}EI\kappa^2. \tag{A.6}$$

The dot symbol implies differentiation with respect to time. Substitution of Eqs. (A.1), (A.4), and (A.5) into Eq. (A.6) leads to

$$\begin{aligned}\mathscr{L} &= \mathscr{L}(\dot{u}, u', \dot{y}, y', \dot{\theta}, \theta') \\ &= \frac{1}{2}\rho A(\dot{u}^2 + \dot{y}^2) + \frac{1}{2}\rho I\dot{\theta}^2 - \frac{1}{2}EA\left[u' + \frac{1}{2}(y')^2 + \frac{1}{2}(u')^2\right]^2 \\ &\quad - \frac{1}{2}EI\left[\frac{(\theta')^2}{(1+u')^2 + (y')^2}\right],\end{aligned} \tag{A.7}$$

where

$$\theta' = \frac{(1+u')y'' - u''y'}{(1+u')^2 + (y')^2}.$$

According to Hamilton's principle, the motion of a beam is such that the integral J of the Lagrangian density has a stationary value, that is,

$$\delta J = \int_{t_1}^{t_2}\int_{x_1}^{x_2} \delta\mathscr{L}\,\mathrm{d}x\,\mathrm{d}t + \int_{t_1}^{t_2}\int_{x_1}^{x_2}(F_u\delta u + F_y\delta y)\,\mathrm{d}x\,\mathrm{d}t + \int_{t_1}^{t_2}\delta W_B\,\mathrm{d}t = 0, \tag{A.8}$$

where

$$\delta\mathscr{L} = \frac{\partial\mathscr{L}}{\partial\dot{u}}\delta\dot{u} + \frac{\partial\mathscr{L}}{\partial u'}\delta u' + \frac{\partial\mathscr{L}}{\partial\dot{y}}\delta\dot{y} + \frac{\partial\mathscr{L}}{\partial y'}\delta y' + \frac{\partial\mathscr{L}}{\partial\dot{\theta}}\delta\dot{\theta} + \frac{\partial\mathscr{L}}{\partial\theta'}\delta\theta'$$

is the variation in the Lagrangian density, $F_{u,y}$ are the external forces, and δW_B is the virtual work performed at the boundaries ($x = x_{1,2}$). Because the tangential angle θ depends on the displacements u and y according to Eq. (A.4), the variations $\delta\dot{\theta}$ and $\delta\theta'$ in $\delta\mathscr{L}$ must be recast in the form

$$\delta\dot{\theta} = \frac{\partial}{\partial t}\left(\frac{\partial\theta}{\partial u'}\right)\delta u' + \frac{\partial}{\partial t}\left(\frac{\partial\theta}{\partial y'}\right)\delta y' + \frac{\partial\theta}{\partial u'}\delta\dot{u}' + \frac{\partial\theta}{\partial y'}\delta\dot{y}', \tag{A.9}$$

$$\delta\theta' = \frac{\partial}{\partial x}\left(\frac{\partial\theta}{\partial u'}\right)\delta u' + \frac{\partial}{\partial x}\left(\frac{\partial\theta}{\partial y'}\right)\delta y' + \frac{\partial\theta}{\partial u'}\delta u'' + \frac{\partial\theta}{\partial y'}\delta y''. \tag{A.10}$$

Solving Eq. (A.8) in conjunction with Eqs. (A.9) and (A.10) yields the following set of equations of motion in the flexural and longitudinal displacements:

$$-\frac{\partial}{\partial t}\left(\frac{\partial\mathscr{L}}{\partial\dot{y}}\right) - \frac{\partial}{\partial x}\left(\frac{\partial\mathscr{L}}{\partial y'}\right) + \frac{\partial}{\partial x}\left\{\left[\frac{\partial}{\partial t}\left(\frac{\partial\mathscr{L}}{\partial\dot{\theta}}\right) + \frac{\partial}{\partial x}\left(\frac{\partial\mathscr{L}}{\partial\theta'}\right)\right]\frac{\partial\theta}{\partial y'}\right\} + F_y = 0, \tag{A.11}$$

$$-\frac{\partial}{\partial t}\left(\frac{\partial\mathscr{L}}{\partial\dot{u}}\right) - \frac{\partial}{\partial x}\left(\frac{\partial\mathscr{L}}{\partial u'}\right) + \frac{\partial}{\partial x}\left\{\left[\frac{\partial}{\partial t}\left(\frac{\partial\mathscr{L}}{\partial\dot{\theta}}\right) + \frac{\partial}{\partial x}\left(\frac{\partial\mathscr{L}}{\partial\theta'}\right)\right]\frac{\partial\theta}{\partial u'}\right\} + F_u = 0. \tag{A.12}$$

The above wave equations with the Lagrangian density given by Eq. (A.7) are valid at all orders (within the framework of geometric nonlinearity), but are not convenient for analysis. Thus, binomial expansion of Eqs. (A.11) and (A.12), following the substitution of Eq. (A.7), is performed to produce equations that are valid up to $O(\varepsilon^2)$. After straightforward (albeit extensive)

algebra, Eqs. (A.11) and (A.12) reduce to

$$\frac{\partial^4 y}{\partial x^4}+\frac{1}{a^2}\frac{\partial^2 y}{\partial t^2}-\frac{1}{c_l^2}\frac{\partial^4 y}{\partial x^2\partial t^2}=\tilde{F}_y(x,t), \tag{A.13}$$

$$\frac{\partial^2 u}{\partial x^2}-\frac{1}{c_l^2}\frac{\partial^2 u}{\partial t^2}=-\frac{1}{2}\frac{\partial (y')^2}{\partial x}-r^2\frac{\partial}{\partial x}[y'y'''-(y'')^2]+\frac{r^2}{c_l^2}\frac{\partial}{\partial x}(y'\ddot{y}')+\tilde{F}_u(x,t), \tag{A.14}$$

where $c_l=\sqrt{E/\rho}$ the longitudinal wave speed, $r=\sqrt{I/A}$ the radius of gyration for the cross-section, $\tilde{F}_y=F_y/EI$, and $\tilde{F}_u=F_u/EA$. Eqs. (A.13) and (A.14) represent, respectively, consistent $O(\varepsilon)$ and $O(\varepsilon^2)$ approximations of the full equations of motion [Eqs. (A.11) and (A.12)] for the flexural and longitudinal vibration of a beam. Nonlinear terms on the right-hand side of Eq. (A.14) are arranged in order of extension, bending, and rotational inertia contributions.

For the purpose of the low-frequency vibration generator under consideration, further simplification of the model equations is necessary. To judge the relative importance of the terms in Eqs. (A.13) and (A.14), the following dimensionless variables are introduced:

$$\overline{x}=\beta x \quad \text{and} \quad \overline{t}=\omega t. \tag{A.15}$$

Here, β is the wave number of a typical mono-frequency wave and ω the corresponding angular frequency. Eqs. (A.13) and (A.14) become, after nondimensionalization,

$$\frac{\partial^4 \overline{y}}{\partial \overline{x}^4}+\left(\frac{1}{1+\Pi}\right)\frac{\partial^2 \overline{y}}{\partial \overline{t}^2}-\left(\frac{\Pi}{1+\Pi}\right)\frac{\partial^4 \overline{y}}{\partial \overline{x}^2\partial \overline{t}^2}=\frac{1}{\beta^3}\tilde{F}_y(x,t), \tag{A.16}$$

$$\begin{aligned}\frac{\partial^2 \overline{u}}{\partial \overline{x}^2}-\left(\frac{\Pi}{1+\Pi}\right)\frac{\partial^2 \overline{u}}{\partial \overline{t}^2}=&-\frac{1}{2}\frac{\partial (\overline{y}')^2}{\partial \overline{x}}-\Pi\frac{\partial}{\partial \overline{x}}[\overline{y}'\overline{y}'''-(\overline{y}'')^2]\\&+\left(\frac{\Pi^2}{1+\Pi}\right)\frac{\partial}{\partial \overline{x}}(\overline{y}'\ddot{\overline{y}}')+\frac{1}{\beta}\tilde{F}_u(x,t),\end{aligned} \tag{A.17}$$

where the bar symbol is used to denote dimensionless quantities, and $\Pi=(\beta r)^2$ is a dimensionless parameter that quantifies the beam thickness relative to the wavelength. From Fig. 2(a), the external force that is to be entered into Eq. (A.16) takes the form

$$\tilde{F}_y(x,t)=-\tilde{c}(\omega)\frac{\partial y}{\partial t}+(\tilde{F}_s+\tilde{F}_d e^{-i\omega t})\delta(x-x_0). \tag{A.18}$$

Now, we invoke the thin-beam assumption [$\Pi=(\beta r)^2\ll 1$] in Eqs. (A.16) and (A.17), and rewrite the resulting equations in terms of physical variables (that is without bar symbols) to arrive at Eqs. (1) and (4).

References

[1] T.R. Licht, S.E. Salboel, Low frequency absolute and comparison calibration of vibration transducers—Uncertainties and challenges, *Proceedings of 2003 NCSL International Workshop and Symposium*, Tampa, August 2003 (available from NCSL International, 2995 Wilderness Place, Suite 107, Boulder, CO 80301-5404), paper 8b-2.

[2] International Organization for Standardization ISO 16063-11:1999, *Mechanical Vibration and Shock—Methods for the Calibration of Vibration and Shock Transducers—Part 11: Primary Vibration Calibration by Laser Interferometry*, 1999.
[3] International Organization for Standardization ISO 16063-21:2003, *Mechanical Vibration and Shock—Methods for the Calibration of Vibration and Shock Transducers—Part 21: Vibration Calibration by Comparison to a Reference Transducer*, 2003.
[4] International Organization for Standardization ISO 16063-1:1998, *Mechanical Vibration and Shock—Methods for the Calibration of Vibration and Shock Transducers—Part 1: Basic Concepts*, 1998.
[5] P.M. Morse, *Vibration and Sound*, American Institute of Physics, New York, 1981, pp. 104–105.
[6] T.J. Anderson, A.H. Nayfeh, B. Balachandran, Experimental verification of the importance of the nonlinear curvature in the response of a cantilever beam, *Journal of Vibration and Acoustics* 118 (1996) 21–27.
[7] J.G. Berry, P.M. Naghdi, On the vibration of elastic bodies having time-dependent boundary conditions, *Quarterly Journal of Applied Mathematics* 14 (1956) 43–50.
[8] K.N. Tong, *Theory of Mechanical Vibration*, Wiley, New York, 1960, pp. 260–271.
[9] K.F. Graff, *Wave Motion in Elastic Solids*, Dover, New York, 1991, pp. 164–165.
[10] L.E. Kinsler, A.R. Frey, A.B. Coppens, J.V. Sanders, *Fundamentals of Acoustics*, third ed., Wiley, New York, 1982 p. 461.
[11] B. Balachandran, Dynamics of an elastic structure excited by harmonic and aharmonic impactor motions, *Journal of Vibration and Control* 9 (2003) 265–279.
[12] T.J. Anderson, A.H. Nayfeh, B. Balachandran, Coupling between high-frequency modes and a low-frequency mode: theory and experiment, *Nonlinear Dynamics* 11 (1996) 17–36.
[13] International Organization for Standardization, *ISO/IEC Guide to the Expression of Uncertainty in Measurement*, Geneva, 1995.
[14] H. Wagner, Large-amplitude free vibrations of a beam, *Journal of Applied Mechanics* 32 (1965) 887–892.
[15] M.R.M. Crespo da Silva, C.C. Glynn, Nonlinear flexural–flexural–torsional dynamics of inextensional beams—I: equations of motion, *Journal of Structural Mechanics* 6 (1978) 437–448.
[16] S.-R. Hsieh, S.W. Shaw, C. Pierre, Normal modes for large amplitude vibration of a cantilever beam, *International Journal of Solids and Structures* 31 (1994) 1981–2014.
[17] C.-H. Ho, R.A. Scott, J.G. Eisley, Non-planar non-linear oscillations of a beam—I: forced motions, *International Journal of Non-Linear Mechanics* 10 (1975) 113–127.
[18] G.R. Bhashyam, G. Prathap, Galerkin finite element method for non-linear beam vibrations, *Journal of Sound and Vibration* 72 (1980) 191–203.
[19] B.S. Sarma, T.K. Varadan, Lagrange-type formulation for finite element analysis of non-linear beam vibrations, *Journal of Sound and Vibration* 86 (1983) 61–70.
[20] E.C. Haight, W.W. King, Stability of nonlinear oscillations of an elastic rod, *Journal of the Acoustical Society of America* 52 (1972) 899–911.
[21] I.S. Raju, G. Venkateswara Rao, K. Kanaka Raju, Effect of longitudinal or inplane deformation and inertia on the large amplitude flexural vibrations of slender beams and thin plates, *Journal of Sound and Vibration* 49 (1976) 415–422.
[22] C. Mei, K. Decha-Umphai, A finite element method for non-linear forced vibrations of beams, *Journal of Sound and Vibration* 102 (1985) 369–380.
[23] D.H. Hodges, Proper definition of curvature in nonlinear beam kinematics, *AIAA Journal* 22 (1984) 1825–1827.